This is an open access article published under a Creative Commons Attribution (CC-BY) License, which permits unrestricted use, distribution and reproduction in any medium, provided the author and source are cited.

ACS AUTHORCHOICE

ACS APPLIED MATERIALS & INTERFACES

www.acsami.org

Research Article

Versatile Phosphate Diester-Based Flame Retardant Vitrimers via Catalyst-Free Mixed Transesterification

Xiaming Feng and Guoqiang Li*

Cite This: *ACS Appl. Mater. Interfaces* 2020, 12, 57486−57496

Read Online

ACCESS | Metrics & More | Article Recommendations | Supporting Information

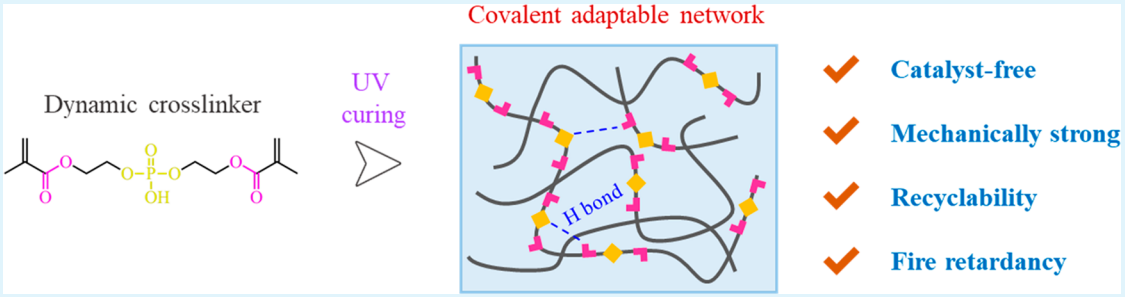

ABSTRACT: We herein report a new vitrimer system integrated with UV curability, recyclability, and flame retardancy. Energy-efficiency, sustainability, and safety have been required features for next-generation polymer materials. Various attempts have been made to endow thermoset polymers with rapid prototyping capacity, recyclability, and flame retardancy. Thermoset vitrimers based on covalent adaptable networks (CANs) are recyclable and remoldable but are generally not UV curable or flame retardant. Here, we present a conceptually novel option to achieve fast exchange reactions in CANs via catalyst-free mixed transesterification of a UV curable phosphate diester-based acrylate cross-linker. In this system, the phosphate diesters serve as reversible covalent bonds, hydrogen bonding ligands, and flame-retardant structures, while acrylate groups serve as UV curable units as well as transesterification collaborators. After the facile UV curing, an intrinsic flame-retardant and mechanically strong dynamic network was achieved due to abundant hydrogen bonds between P−OH and C═O structures. Additionally, this highly cross-linked network exhibited an attractive recyclability even at temperatures lower than T_g. This phosphate diester-based mixed transesterification concept represents an efficient approach for developing multifunctional vitrimers and can also be generalized into other thermally cured polymer systems.

KEYWORDS: *phosphate diester, vitrimer, recyclability, flame retardancy, mixed transesterification*

INTRODUCTION

With the advancement in polymer materials science and technology, the desire for polymers to be manufactured rapidly and used sustainably and safely is increasingly becoming strong, and the target has kept rising. To satisfy these ever-increasing requirements, three separated research directions, i.e., UV curable polymers, recyclable thermoset polymers, and flame-retardant polymers, were created and progressed rapidly. However, in modern applications, it is required that polymers have multifunctionalities such as rapid prototyping, recyclability, and flame retardance simultaneously. Up to now, some studies have tried to address two of the three requirements at the same time, such as the development of UV curable and recyclable thermoset polymers,[1−3] and UV curable and flame-retardant coatings.[4,5] To the best of our knowledge, there is no report on polymers integrated with the three properties within one polymer network. Therefore, it is highly desired to develop new polymer materials which have the three required features simultaneously.

Recently, various dynamic covalent bonds were explored to achieve covalent adaptable networks (CANs) in developing recyclable thermoset polymers, or vitrimers, the cross-linked networks of which can reform and rearrange upon the external stimulus, e.g. thermal or light.[6,7] This dynamic nature makes the resulted vitrimer be malleable, recyclable, and reprocessable. So far, there are two major categories, dissociative and associative bond exchanges. More than ten different reversible covalent bonds have been reported for the fabrication of vitrimers, such as Diels−Alder reaction,[8] urethane/urea dissociation,[9] transalkylation,[10] transamination,[11] disulfide exchange,[12] Michael adduct exchange,[13] transesterification,[14]

Received: October 20, 2020
Accepted: December 7, 2020
Published: December 11, 2020

© 2020 The Authors. Published by American Chemical Society

Scheme 1. (a) Schematic Structure of RNA and Its Cleavage via Internal Transesterification and (B) Possible Mixed Transesterification between Phosphate Diester Catalyst and Carboxylate Esters

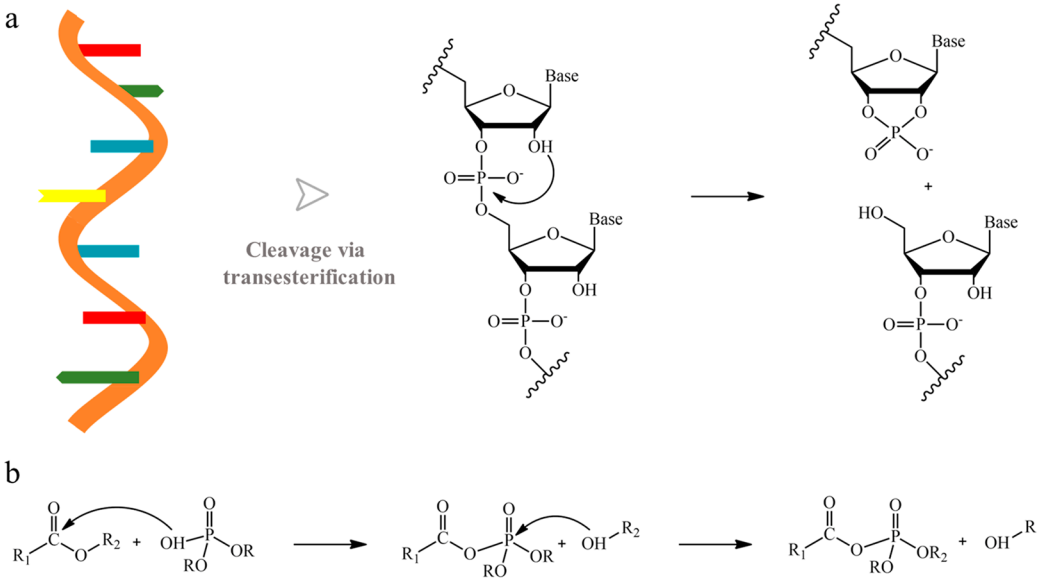

olefin metathesis,[15] dioxaborolane metathesis,[16] transthioetherification,[17] and silyl ether exchange.[18] Despite the great significance to the advancement in scientific understanding, some of them are limited by their complicated synthesis, usage of expensive or toxic catalyst, and fair mechanical performance for practical applications. Notably, all of these reversible covalent bonds are single-function for achieving dynamic networks, and none of them is intrinsically flame retardant. To endow the CANs with flame retardancy, the major challenge lies in the difficulty in finding the right combinations of recyclability and flame retardancy. In those few reports that tried to achieve recyclability and flame retardancy simultaneously,[19,20] they all followed a complicated and costly synthesis route by including extra flame-retardant additives/structures into the existing dynamic thermoset networks. Therefore, new reversible covalent chemistry that can ensure intrinsic flame safety while maintaining excellent dynamic ability must be sought.

Phosphate diesters are well-known for serving as the linkages between neighboring bases in RNA and DNA. Due to the chemical stability, they are chosen by nature to achieve long-term storage of genetic information. The phosphate diester transesterification has been identified for the modification and cleavage of RNA for a long time (Scheme 1a).[21,22] Various complex catalysts were developed for accelerating the transesterification process.[23−25] However, most of them were conducted in the biological surroundings (specific pH and enhydrous environments). The dynamic exchange process of phosphate diesters within polymer materials has rarely been reported before. It is known that the catalytic action of phosphate diesters in the controlled ring-opening polymerization of cyclic esters has been well-established.[26,27] Shaver et al. reported a deactivation pathway for phosphate diester catalysts because of the ester exchange between P−OH of phosphate diesters and β-butyrolactone,[28] which indicates the possible mixed ester exchange process between phosphate diesters and conventional carboxylate esters (Scheme 1b). In addition, different from conventional flame retardants such as toxic halogenated flame retardant[29] and inefficient inorganic layered flame retardants,[30,31] the small phosphate ester molecules have been widely studied and used as environmentally friendly flame retardants for polymeric materials because of their unique thermal decomposition pathway.[32−34] Based on the above analysis, the dynamic phosphate diester chemistry shows great potential for development of recyclable thermoset networks with intrinsic flame retardancy.

In this work, for the ease of use in practical applications, we rediscovered a commercially available dimethacrylate monomer containing phosphate diester structure, bis[2-(methacryloyloxy)ethyl] phosphate (BPA). Due to the mixed transesterification of the embedded phosphate diesters and carboxylate esters of acylate structures, the facilely UV cured BPA thermoset networks exhibited a fantastic dynamic nature. Benefiting from the initial high strength and rapid exchange reactions, a considerably strong polymer network was recycled under moderate conditions. Further, the abundant phosphate diester structures endowed the BPA networks with intrinsic flame retardancy. The detailed flame-retardant mechanism was systematically investigated with the help of morphology and structure characterization techniques.

RESULT AND DISCUSSION

Preparation and Mechanical Properties. To illustrate the mixed ester exchange concept better, in this work, we chose a conventional UV curable cross-linker, 1,6-hexanediol dimethacrylate (HDA), as the reference. As shown in Figure S1, the clear HDA monomer and photoinitiator solution cross-linked into a bulk polymer after UV exposure, and a rupture caused by dramatic shrinkage can be observed for the UV cured HDA sample. The obvious absorption peaks (1636 cm^{-1}, 814 cm^{-1}) ascribed to residual C═C bonds in FTIR spectrum (Figure S2) also indicate the poor curing performance of the commonly used HDA cross-linker. In comparison, the BPA monomer was well-cured under the same conditions according to the almost disappeared absorption peaks of C═C bonds, and no obvious shrinkage occurred during the UV curing process. The acrylate double bond (C═C) conversions of the BPA and HAD samples were calculated to be 82.6 and

https://dx.doi.org/10.1021/acsami.0c18852
ACS Appl. Mater. Interfaces 2020, 12, 57486−57496

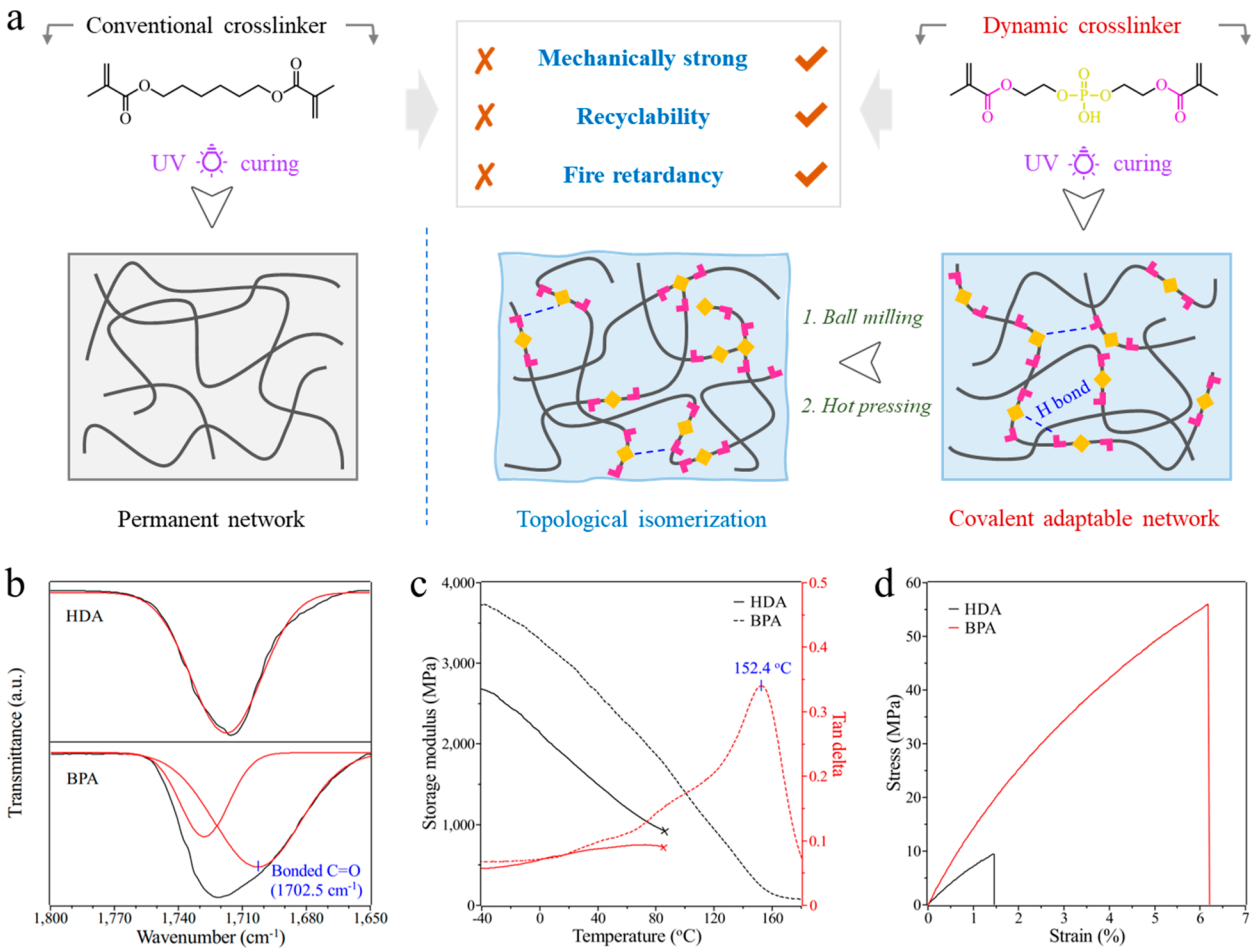

Figure 1. (a) Schematic illustration of the performance comparison between the conventional cross-linker and the dynamic phosphate diester-based cross-linker. The yellow blocks represent the dynamic phosphate diester bonds, and the pink "L-shaped" blocks represent carboxylic esters as the mixed transesterification collaborator. (b) FTIR spectra of the UV cured HDA and BPA in the range of 1800−1650 cm^{-1} assigned to the characteristic absorption peak of the C═O group. (c) Storage modulus and tan δ curves, and (d) representative plots of the tensile stress vs tensile strain curve of the UV cured HDA and BPA.

68.6%, respectively, according to the area ratios of the absorption peak around 814 cm^{-1} before and after curing. The obtained BPA thermoset polymer is light pink color with high transparency.

The performance comparison between the conventional HDA cross-linker and the dynamic BPA cross-linker is illustrated in Figure 1a. Owing to the lack of free hydroxyl groups, the carboxylic esters in the HDA structure cannot achieve the ester exchange reaction nor the formation of hydrogen bonding. The resulted HDA thermoset polymer possesses a permanent cross-linked network with only fair mechanical properties. Notably, the HDA sample was broken around 90 °C during the dynamic mechanical test (marked with a cross mark in Figure 1c), indicating its poor dynamic mechanical performance. In contrast, due to the presence of phosphate diesters, the P−OH groups interacted with C═O bonds of carboxylate esters and formed abundant hydrogen bonds within the BPA networks, which can be confirmed by the FTIR absorption peak of bonded C═O structures (Figure 1b).[35] These abundant hydrogen bonds together with the high glass transition temperature (T_g) (152.4 °C) and high cross-linking density (7.1 × 10^3 mol/m^3) lead to a mechanically robust thermoset network (Figure 1c). Figure 1d compares the tensile stress−strain curves of the HDA and BPA samples. The tensile strength and elongation at break of the HDA networks are around 10 MPa and 1.5%, respectively; while the tensile strength and elongation at break of the BPA sample can reach 54.6 MPa and 7.5%, respectively. Further, the compression experiments of BPA samples also demonstrated excellent compressive property even at elevated temperatures (Figure S3). These results indicate that the BPA cross-linker is much better in fabricating high-strength UV cured thermoset polymers. Moreover, benefiting from the dynamic nature and particular thermal decomposition behavior of phosphate diesters, the BPA networks are expected to show high recyclability and flame retardancy, which is discussed in the following sections.

Rheological Analysis. Before the thermal recycling experiments, the rheologies of the HDA and BPA networks were evaluated using a dynamic mechanical analyzer (DMA). The stress relaxation tests were performed first to characterize the nature of each network. Figure 2a, b shows the stress decay over time when a constant strain within the linear viscoelastic regime was applied to the HDA or BPA samples, respectively. Obviously, after an initial drop caused by the limited segment motion, the stress of the HDA sample upon stretching was quite stable, which means the permanent cross-linked networks cannot reconstruct and rearrange to relax the external force. In

https://dx.doi.org/10.1021/acsami.0c18852
ACS Appl. Mater. Interfaces 2020, 12, 57486−57496

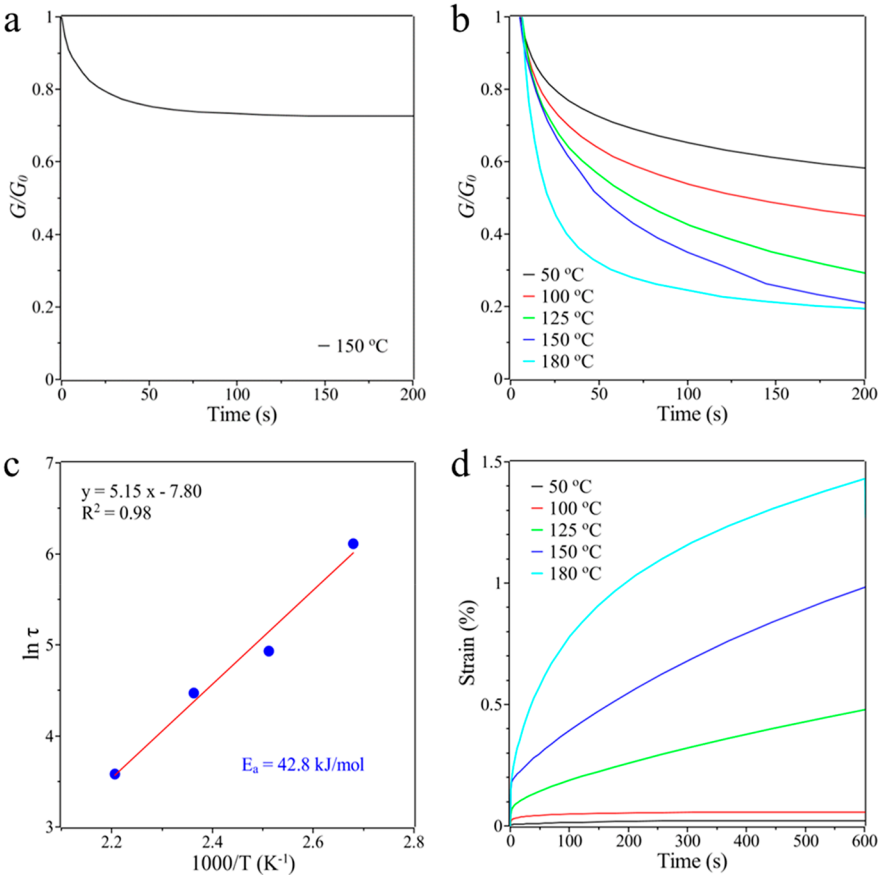

Figure 2. Normalized stress relaxation curves of (a) HDA at 150 °C and (b) BPA at different temperatures. (c) Arrhenius plot to calculate the activation energy (E_a) and (d) creep strain of BPA at different temperatures while maintaining a constant stress.

contrast, the BPA network followed an exponential Maxwell stress decay and rapidly relaxed the external load, suggesting its dynamic nature. When the relaxation temperature increases, the stress decay becomes faster. The characteristic relaxation time (τ^*), which is defined as the time that stress decays to 1/e of the initial stress, was utilized to compare relative stress−relaxation rates at different temperatures. For example, the τ^* of BPA networks at 125 °C is 138 s, while it takes only 37 s at 180 °C. By substituting the τ^* values at different temperatures (K) into the Arrhenius equation, the slope of the Arrhenius plot ($\ln(\tau)$ vs $1000/T$) can be used to determine the activation energy (E_a) of the dynamic BPA networks.[14,18] It is calculated to be 42.8 kJ/mol under catalyst-free conditions, which is lower than that of most previously reported dynamic thermoset networks, although some of them have been accelerated by catalysts.

Besides T_g, the topology freezing transition temperature (T_v), at which the viscosity η is 10^{12} Pa·s, is defined as the temperature at which the network topology is frozen through kinetic trapping of its internal dynamic chemistry.[18] The T_v of the BPA network is calculated to be 9.1 °C, which is far below the T_g. This demonstrates that the dynamic behavior of the BPA network is primarily controlled by segments motion, namely glass transition. Once the segments motion occurs, the networks can achieve conformational adjustment and topological isomerization through the rapid dynamic phosphate diesters exchange chemistry, as well as through endowing the resulted thermoset polymer with high thermal malleability. Additionally, the BPA networks were subjected to creep experiments at elevated temperatures (Figure 2d). A negligible strain creep below 100 °C can be observed, which suggests good dimensional stability in practical applications. When the temperature was close to the T_g, the BPA network showed an increased creep after the initial elastic response. As expected, the BPA network displayed more creep at higher temperature due to the temperature-dependent phosphate diester exchange reaction. Furthermore, the usage of BPA monomers as dynamic cross-linker for conventional methyl acrylate (MA) and butyl acrylate (BA) can also lead to strong and highly adaptable cross-linked networks (Figure S4), both of which showed fast stress relaxation performance. These results indicate that the dynamic BPA cross-linker can be applied to fabricate various UV curable CANs by modifying the compositions and formulations.

Thermal Recycling. The great advantage of dynamic cross-linked network over permanent cross-linked network is the reprocessability or recyclability of the resulted thermoset polymers. In this work, a simple hot-pressing method was performed to examine the recyclability of the phosphate diester-based dynamic networks. As shown in Figure 3a, the BPA samples were first milled into powders (Figure S5) and then hot pressed into a new transparent bar specimen due to the dynamic network feature. In comparison, the HDA powders with permanent cross-linked network were totally incapable of recycling by hot pressing under the same conditions (Figure 3b). The recycling procedures of the BPA samples were conducted under different time and temperature conditions and the recycled samples were characterized with a

https://dx.doi.org/10.1021/acsami.0c18852
ACS Appl. Mater. Interfaces 2020, 12, 57486−57496

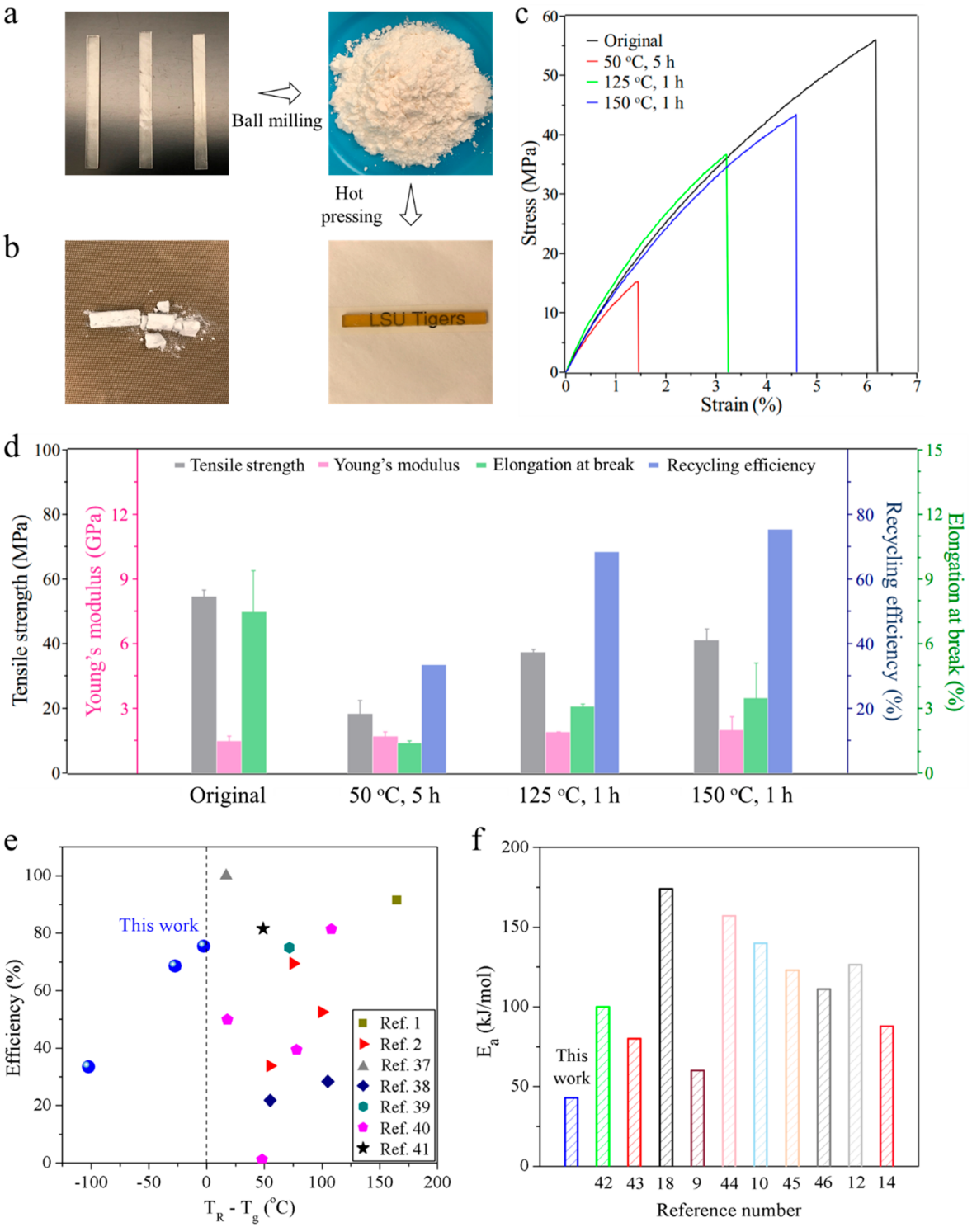

Figure 3. (a) Physical recycling of the BPA thermoset through ball milling the broken sample and hot pressing the milled powders. (b) The obtained sample of the HDA after the sample recycling procedure. (c) Tensile stress−strain curves of the original and recycled BPA thermoset under varying recycling conditions. (d) Tensile strength, Young's modulus, elongation at break, and recycling efficiency of the original and recycled BPA samples. (e) Comparison of the recycling efficiency and difference between T_g and recycling temperature (T_R) of BPA with those of previously reported recyclable UV cured thermosets. (f) Comparison of activation energy (E_a) of the BPA with previously reported dynamic exchange reaction (thiol-thioester,[42] boroxine,[43] silyl ester,[18] amine,[9] imine,[44] salkylation,[10] carbonation,[45] carbamate,[46] disulfide,[12] and carboxylate ester[14])-based thermosets.

tensile test. Figure 3c displays the representative stress−strain curves of the intact and recycled BPA samples, and characteristic indicators are summarized in Figure 3d and Table S2. Obviously, the recycling efficiency was improved with the increase in reprocessing temperature. The tensile strength and Young's modulus of the specimen recycled at 150 °C for 1 h under the pressure of 10 MPa can reach 41.2 MPa and 2.0 GPa, respectively. The recycling efficiency defined as

https://dx.doi.org/10.1021/acsami.0c18852
ACS Appl. Mater. Interfaces 2020, 12, 57486−57496

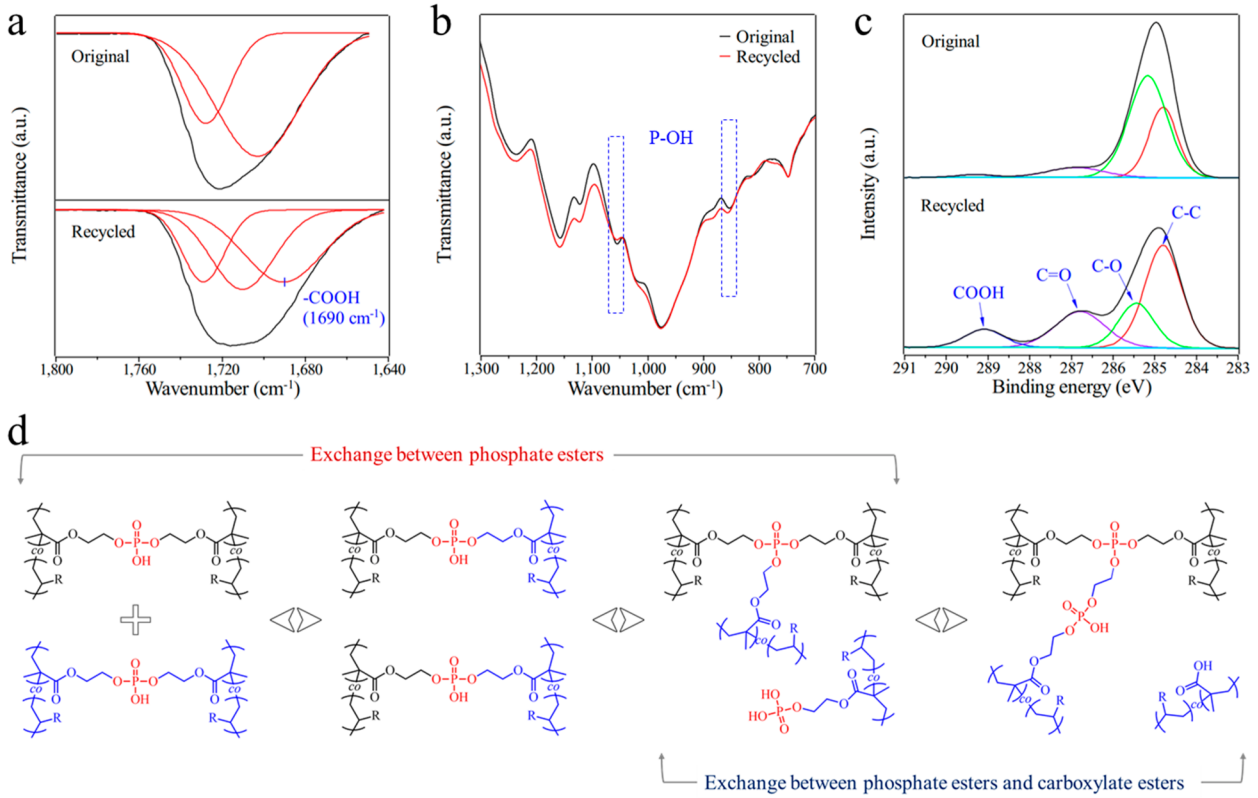

Figure 4. (a, b) Enlarged FTIR spectra and (c) high-resolution C 1s XPS spectra of the original and recycled BPA samples. (d) Mixed exchanges of phosphate diester-based cross-linker generated dynamic thermosets. The black and blue colors represent the two different molecular chains that take part in the transesterifcation process within the BPA networks.

the ratio of tensile strengths before and after recycling was calculated to be 75.5%, which is acceptable in consideration of the high T_g (152.4 °C) and high tensile strength of the intact sample (Table S1). Notably, the Young's modulus of the recycled specimen was completely recovered. Almost the same smooth fracture surfaces (Figure S6) demonstrated the typical brittle rupture behavior of both the original and recycled BPA thermosets. It reveals that the simple hot-pressing recycling could revert to a large extent to the original mechanical performances. Meanwhile, isothermal and nonisothermal TG curves under nitrogen and air atmosphere indicate that the phosphate diester-based dynamic network was thermally stable up to 200 °C, which is higher than the above-mentioned recycling temperature (150 °C) (Figures S7 and S8).

Compared to thermally induced polymerization, it is widely reported that UV photopolymerization of acrylates can lead to a denser cross-linked network because of more chain transfer reactions to macromolecules.[36] For these dynamic acylate monomers, they make a portion of the permanent cross-linked networks exist in the resulting dynamic thermoset network (Figure S9) or interpenetrated network. Different from the thermally condensed dynamic networks, these permanent cross-linked networks, together with the radical polymerized long chain which has low mobility, always generate a considerable reduction in the recycling efficiency. In Table S3, we summarized the recycling conditions and recycling efficiency of previously reported UV cured dynamic thermosets. Obviously, the recycling efficiencies of most reported systems are lower than 82%. Indeed, Zhang et al. reported a 3D printed system with recycling efficiency around 91.5%,[1] which is mainly attributed to its low T_g (55 °C) and low tensile strength, as well as the extremely rigorous recycling conditions (220 °C, 500 MPa pressure for 2 h). Most recently, Huang et al. developed a UV cured dynamic thermoset with 100% recycling efficiency.[37] This fantastic mechanical recoverability is partially caused by the dissociative Diels−Alder coupling-based de-cross-linking action of networks at high temperature. However, they recycled the samples at 130 °C for 1 h and then at 80 °C for another 24 h, which is much more time-consuming and costly in practical applications.

Figure 3c shows the comparison of the recycling efficiency and the difference between the T_g and recycling temperatures of BPA samples with those of previously reported recyclable UV cured thermosets.[1,2,37−41] Obviously, the BPA thermoset possesses a comparable recycling efficiency while exhibiting a glassy state recyclability. Even when the recycling temperature is 27.4 °C lower than the T_g, the recycling efficiency is still close to 70% under an easily achieved 10 MPa pressure and for only 1 h. This promising performance is primarily caused by the wide glass transition region and much lower T_v compared to T_g, which means the dynamic ester exchanges can rapidly occur even when most chain segments are frozen. Figure 3f compared the E_a value of the BPA system with previously reported dynamic exchange reaction-based thermosets. The BPA system shows the lowest E_a value, which suggests that the exchange reaction can occur easily because of the lower energy barrier. Most importantly, some of those existing exchange reactions rely heavily on the addition of external catalyst for obtaining an acceptable exchange rate, such as carboxylate ester exchange, carbonation exchange, silyl ether exchange, and thiol-thioester exchange. In contrast, there is no requirement for catalyst for the phosphate diester exchange reaction in the

https://dx.doi.org/10.1021/acsami.0c18852
ACS Appl. Mater. Interfaces 2020, 12, 57486−57496

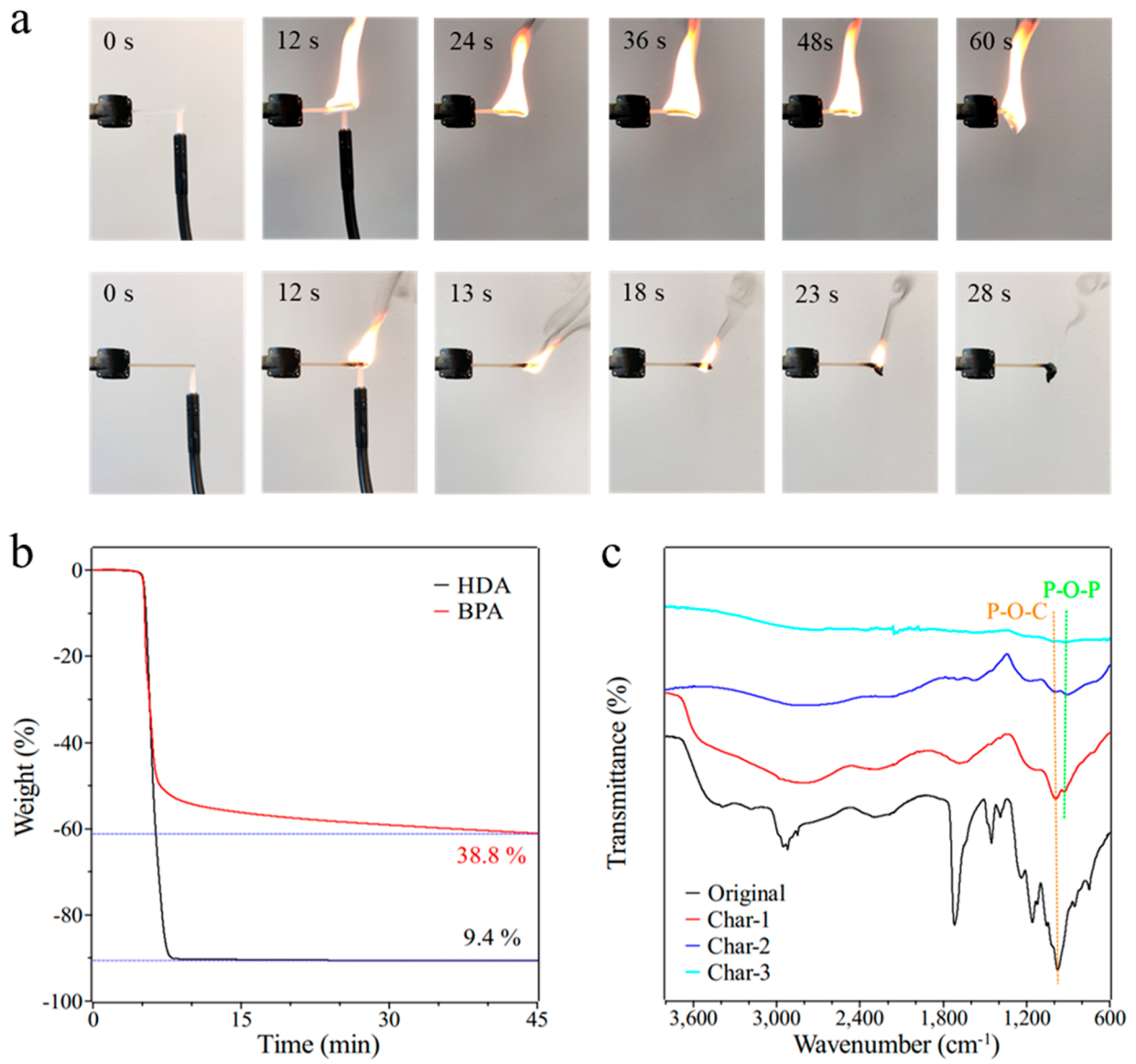

Figure 5. (a) Combustion performance of the HDA (top) and the BPA (bottom) specimens. (b) TG curves of the HDA and the BPA samples isothermal at 485 °C for 45 min. (c) FTIR spectra of the char residue at different positions of BPA after combustion testing.

BPA networks. This rapid exchange reaction leads to efficient topology arrangement of cross-linked networks as well as the good thermal recycling performance.

Mixed Transesterification Mechanism. FTIR and XPS spectra were performed to explore the mixed transesterification during recycling of the BPA network. Figure S10 displays the FTIR spectra of the original and recycled BPA samples. The similar absorption curves before and after recycling suggested that no obvious thermal degradation occurred. A new fitted absorption peak around 1690 cm^{-1} is presented in the enlarged FTIR spectra (Figure 4a), which indicates the formation of COOH group after the thermal recycling process.[47,48] A slight decrease in the intensities of the two P−OH absorption peaks demonstrates the consumption of P−OH bonds when the BPA network took the topologic isomerization (Figure 4b). Additionally, the high-resolution C 1s XPS spectra in Figure 4c also confirmed the presence of a COOH structure within the rearranged BPA network after the thermal recycling process. Based on the above experimental results and the previous reports,[28,49] a mixed transesterification of the phosphate diester-based BPA dynamic networks is outlined in Figure 4d. Further, the conventional exchange between phosphate diester themselves, the exchange between phosphate diesters and carboxylate esters might occur when the BPA powders were compressed together. Notably, the mixed transesterification proposed in this work is different from the previous reports as described in the Introduction (Scheme 1b). In those reports, the consumption of one P−OH group leads to the formation of O═C−O−P structure and a new C−OH group. In contrast, here, one P−OH group was replaced by a COOH group after the rearrangement and isomerization of the BPA dynamic network. This difference may be caused by the distinct reaction environments. During the solid recycling process, the movement of chain segments is heavily limited, and the reaction possibility is far lower than that in the liquid phase. This difference between solid phase reaction and liquid phase reaction is common in chemical synthesis. It is worth mentioning that, for the sake of disclosing the exchange mechanism (mode-of-action) between phosphate diesters and carboxylate esters, more systematic studies such as a small-

https://dx.doi.org/10.1021/acsami.0c18852
ACS Appl. Mater. Interfaces 2020, 12, 57486−57496

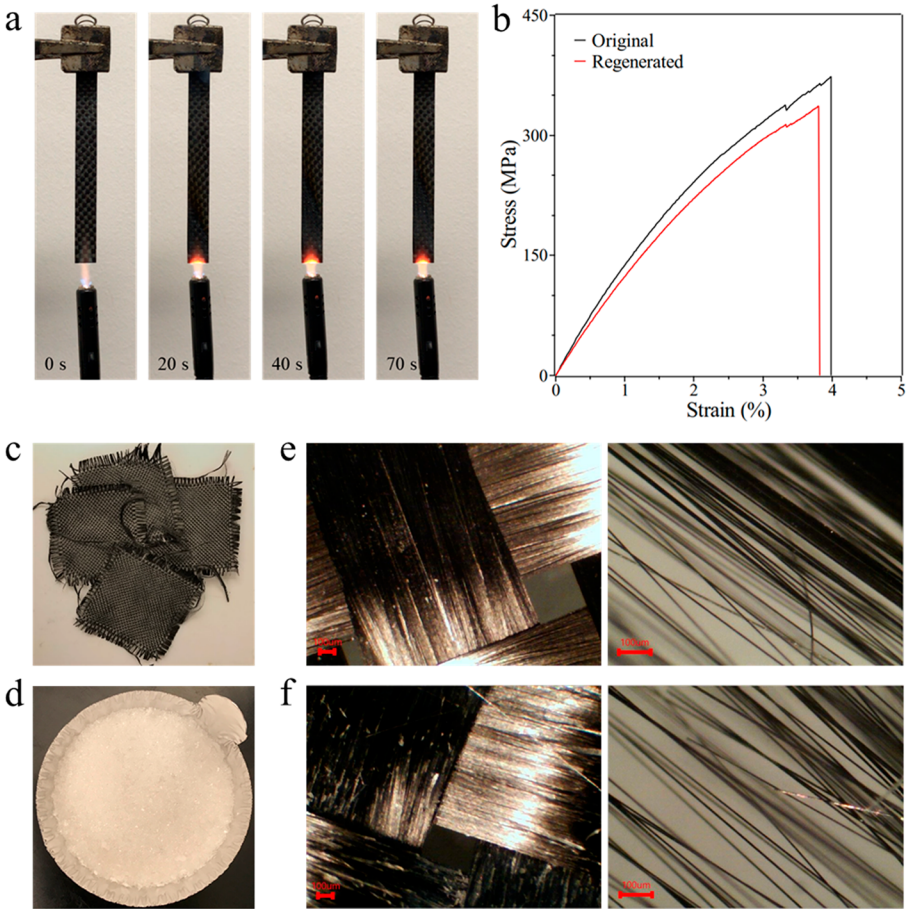

Figure 6. (a) Combustion performance of carbon fiber reinforced BPA composite sample. (b) Tensile stress−strain curves of original BPA composite and regenerated BPA composite. (c) Chemically recycled woven carbon fabric and (d) degraded product of the BPA matrix. Optical microscope images of (e) original woven carbon fabric and (f) recycled woven carbon fabric under different magnifications.

molecule model experiment should be conducted, which will be a topic of research in our future work.

Flame Retardancy. Besides the promising dynamic nature, the specific thermal decomposition behavior of phosphate esters makes them widely studied flame retardants for improving flame retardancy of polymers. However, most of these reports focused on the evaluation of phosphate triesters; only a few works were involved with the investigation of phosphate diesters, such as the capacity of DNA as a bio-based flame retardant.[50] Figure 5a displays the combustion processes of the HDA and BPA samples. Like most polymers, the HDA sample burned vigorously in the air after 12 s ignition and burned out completely. There was little char residue left, which demonstrates that the HDA sample is completely burned and its flame retardancy is almost zero. In contrast, the burning flame of the BPA was much smaller after the same 12 s ignition. The flame was getting increasingly smaller over time and was extinguished after 15 s, which shows high flame retardancy. In addition, an intumescent char residue can be observed on the sample. It is noted that the limiting oxygen index (LOI) and UL-94 tests should be conducted to fully evaluate the flame retardancy of the BPA samples, which will be a topic for our future studies.

Thermogravimetric analysis (TGA) was performed to further characterize the charring capability of these UV cured thermoset polymers (Figure 5b). The BPA sample shows up to 39% residual weight after being thermally degraded at 485 °C for 40 min, while the HDA sample is only 9.4% under the same conditions. Obviously, the charring efficiency of the BPA sample is much higher than that of HDA sample, indicating that the incorporation of phosphate diesters can significantly change the decomposition process of ordinary acylate structures. SEM images were taken to confirm the charring ability of the BPA network (Figure S11). A compact surface structure and cellular inner structure of the BPA char residue can be clearly observed. EDS results demonstrated the gathering of phosphorus in the BPA char residue, indicating the condensed phase flame retardant mechanism.

FTIR spectra were used to evaluate the evolution of the molecular structures during the combustion process. As shown in Figure 5c, the initial BPA sample shows a strong absorption peak around 980 cm^{-1}, which is assigned to the P−O−C bonds. With the occurrence of combustion, the peak intensity of P−O−C bonds continued to decrease, demonstrating the early decomposition of phosphate diester structures. Meanwhile, around 930 cm^{-1}, a new absorption peak ascribed to P−O−P bonds was identified and became stronger relative to the decreased P−O−C bonds. This result suggests that phosphate diesters decomposed first and then condensed into charred phosphoric acid structures as well as the condensed phase flame retardant mechanism. XPS spectra of the original and burnt BPA samples were obtained to further confirm this condensed phase mechanism (Figure S12). As summarized in Table S4, the atomic percentage of P 2p in the char residue is

https://dx.doi.org/10.1021/acsami.0c18852
ACS Appl. Mater. Interfaces 2020, 12, 57486−57496

much higher than that in the intact sample. This means most of the phosphorus elements were condensed in the residual char phase other than in the escaped gas phase. The XPS survey spectra and high-resolution XPS spectra of each elements display the surface chemistry and the bonding characteristics. The O 1s peaks centered at 533.9 and 532.4 eV are attributed to C═O/P═O, and C−O/P−O and P−O−P/C−O−P, respectively.[51,52] The two peaks in the P 2p spectrum at 136.1 and 135.3 eV are assigned to PO_3 and P−O−P structures in the phosphorus-rich cross-linked char, which implies the cross-linking and charring abilities of the embedded phosphate diesters during the thermal decomposition of UV cured BPA polymer.

Chemical Stability and Recyclability of Fiber Reinforced BPA Composites. It is noted that the BPA is quite stable under chemical attacks by various organic solvents, see Figure S13 and Table S5. After 4 days of immersion in organic solvents, including ethanol, acetone, chloroform, toluene, hexanes tetrahydrofuran (THF), ethylene glycol (EG), and dimethylformamide (DMF), almost no changes were found. In addition, we can see some bubbles attached on the surface of the BPA sample after 4 days water immersion test, which indicates that the BPA sample might be degraded in water and shows the possibility of environmental-friendly water-assisted recyclability. Furthermore, the BPA can be cured not only by UV light, but also thermally. As shown in Figure 6, woven carbon fabric was used to reinforce the BPA to form fiber reinforced cross-ply composite with 57% fiber weight fraction and was cured thermally. The composite shows excellent flame retardancy (Figure 6a), high tensile strength up to 370 MPa (Figure 6b), and most importantly, recyclability. As shown in Figure 6c, d, most of the BPA matrix degraded into small particles after the treatment by hot NaOH aqueous solution and can be washed away to recycle the valuable carbon fiber. The similar optical and SEM images of the original and recycled carbon fibers demonstrate that there is no obvious damage on the structure of carbon fibers during the recycling process (Figure S14). Moreover, the recycled carbon fibers can be used to reinforce the BPA material again. The regenerated cross-ply composite still has a tensile strength over 330 MPa (Figure 6b).

CONCLUSIONS

In conclusion, we reported a new type of CAN with fast exchange reaction via the catalyst-free mixed transesterification between phosphate diesters and carboxylate esters. A commercialized dimethacrylate monomer BPA was applied to illustrate this mixed transesterification strategy. After UV curing, the resulting high cross-linking density and the abundant hydrogen bonds between P−OH and C═O groups endowed the BPA network with a considerably high T_g and strong mechanical performance. The stress relaxation behavior with the E_a of 42.8 kJ/mol demonstrated the promising dynamic capability of the BPA network. Due to the low T_v and the broad glass transition region, the BPA network exhibited an attractive thermal recyclability even though the recycling temperature was lower than T_g. The tensile strength of the optimal recycled sample can reach 41.2 MPa. In addition, the dynamic phosphate diesters could make the CANs with intrinsic flame retardancy without the addition of external flame-retardant structures. A condensed phase flame retardant mechanism was established through the high char residue after isothermal degradation and its FTIR and XPS spectral analysis. The dynamic phosphate diester chemistry proposed here is a fantastic drop-in technology that can be easily used to develop a broad range of high-performance CANs while possessing intrinsic flame retardancy.

EXPERIMENTAL SECTION

Materials. 1,6-Hexanediol dimethacrylate (≥90%), bis[2-(methacryloyloxy)ethyl] phosphate, butyl acrylate (≥99%), methyl acrylate (99%), 2-hydroxy-2-methylpropiophenone (97%), sodium hydroxide (NaOH, ≥ 98%), acetone, and lauroyl peroxide (98%) were purchased from Sigma-Aldrich and used as received.

Fabrication of UV Cured Thermosets. The 97 wt % 1,6-hexanediol dimethacrylate or bis[2-(methacryloyloxy)ethyl] phosphate monomers and 3 wt % photoinitiator 2-hydroxy-2-methylpropiophenone was mixed by stirring at room temperature and degassed in a vacuum oven. The homogeneous liquids were poured into a PTFE spacer with thickness of 1.1 mm clamped by two transparent plastic slides. The monomers were then cured in a UV chamber (IntelliRay 600, Uvitron International, United States) for 1 min under 50% irradiation intensity (232 nm, around 65 mW/cm^2 according to the information from the equipment manufacturer). The UV cured samples were obtained by removing the two plastic slides and the PTFE spacer. The cured 1,6-hexanediol dimethacrylate and bis[2-(methacryloyloxy)ethyl] phosphate samples are abbreviated as HDA and BPA, respectively. For using bis[2-(methacryloyloxy)ethyl] phosphate as cross-linker, bis[2-(methacryloyloxy)ethyl] phosphate and butyl acrylate or methyl acrylate in mole ratio of 1:1, and 3 wt % photoinitiator 2-hydroxy-2-methylpropiophenone were mixed at room temperature and degassed in a vacuum oven. Then, the UV curing process is the same as that for preparing pure BPA sample. The obtained samples are abbreviated as BPA-BA and BPA-MA, respectively.

Preparation of Carbon Fiber Reinforced BPA Composites. The 95.5 wt % bis[2-(methacryloyloxy)ethyl] phosphate monomer and 4.5 wt % thermal-initiator lauroyl peroxide were mixed into a homogeneous solution by stirring at 60 °C and then degassed in a vacuum oven. The carbon fiber reinforced BPA composite was prepared by hand applying the homogeneous solution onto 4 layers of woven carbon fabric and then hot-pressing them into 1 mm of thickness between 2 aluminum foils at 100 °C for 2 h. The final sample was obtained by peeling off the aluminum foils and cutting away the edges. The weight fraction of carbon fabric in the BPA composite is around 57%. The regenerated carbon fabric reinforced BPA composite was prepared by the same method except for the usage of recycled woven carbon fabric.

Recycling Experiment. In a physical hot-pressing recycling experiment, first, the UV cured samples were manually broken into small pieces and then ground by a planetary ball mill machine to prepare powders (Across International PQ-N2 Planetary, Livingston, United States). The rotate speed is 400 rpm, and milling time is 2 h. Then, 1 g of milled powder was poured into a steel mold (60 × 5 mm^2) and compressed through a pushing bar under a constant pressure about 10 MPa. Various recycling conditions (150 or 125 °C for 1 h, or 50 °C for 5 h) were set to obtain the recycled samples. The recycling efficiency was calculated by the ratio of tensile strength of the recycled sample to that of the original sample. The chemical recycling process of carbon fabric reinforced BPA composite was conducted by immersing the intact composite plate in 0.5 mol/L NaOH aqueous solution at 100 °C for 12 h. Then, the dissociated woven carbon fabric layers were ultrasonically cleaned in 0.5 mol/L fresh NaOH aqueous solution by an ultrasonic cleaning machine (Branson 3510) at 60 °C for another 12 h. The obtained woven carbon fabric was washed with deionized water five times and naturally dried in a hood.

Characterization. Fourier transform infrared spectroscopy (FTIR) spectra were tested by a Nicolet 6700 FTIR spectrometer (Thermo Fisher Scientific, United States) using the attenuated total reflection mode by collecting 32 scans from 500 to 4000 cm^{-1}. Storage modulus, loss modulus, and tan δ curves were characterized

https://dx.doi.org/10.1021/acsami.0c18852
ACS Appl. Mater. Interfaces 2020, 12, 57486−57496

by a Q800 dynamic mechanical analyzer (DMA) (TA Instruments, DE, United States) in multifrequency strain mode with a heating rate of 3 °C min^{-1} and a frequency of 1 Hz. For stress relaxation, the specimen (25.03 × 5.23 × 1.75 mm^3) was preloaded with 0.001 N force to maintain straightness and equilibrated at 50, 100, 125, 150, and 180 °C for 30 min, respectively. The sample was then stretched and remained a constant strain. The stress value was recorded over time. Creep experiment was monitored by using the Q800 dynamic mechanical analyzer. The sample (24.63 × 5.43 × 1.52 mm^3) was equilibrated for 15 min at specified temperatures (50, 100, 125, 150, and 180 °C) and then pulled by a constant stress (0.1 MPa) and held for 10 min. The strain increasing was recorded over time. Nonisothermal thermogravimetric analysis (TGA) curves were performed using a Q5000 thermal analyzer (TA Co., United States) from 20 to 500 °C at a heating rate of 10 °C/min in both argon and air atmosphere. For isothermal experiments, the sample was rapidly heated from room temperature to the target temperature at a heating rate of 100 °C/min in argon atmosphere, then isothermal for a certain time. The purging rate of the argon gas was 100 mL min^{-1}. The morphologies of carbon woven fiber and ball milled powders were observed by an optical microscope (AmScope MD35) that is connected to a computer for capturing the images. The tensile and compression properties were evaluated by using an eXpert 2610 MTS (ADMET, Norwood, MA, United States) equipped with a temperature-regulated oven. As for the compression test, the compression rate was 0.5 mm/min. The cylindrical samples (height: 11.15 mm, diameter: 8.75 mm) were compressed at 20, 150, 165, and 180 °C, respectively. As for the tensile test, the stretching rate was 1.0 mm/min. The sample plates were sawed into rectangular bars (59.95 × 5.00 × 2.30 mm^3). At least three parallel samples were performed for tensile tests. The flame retardancy of HDA, BPA, and its composite were evaluated by igniting them with a gas burner, and the combustion processes were recorded by a camera. The char residue was collected for further analysis. The XPS spectra were carried out by the Scienta Omicron ESCA 2SR X-ray Photoelectron Spectroscope.

■ ASSOCIATED CONTENT

Supporting Information

The Supporting Information is available free of charge at https://pubs.acs.org/doi/10.1021/acsami.0c18852.

Preparation and characterization information including FTIR, TG, SEM, XPS, compressive test, dissolution experiments, and summary of recycling properties (PDF)

Video of the combustion process of the control HDA thermoset polymer (MP4)

Video of the combustion process of the flame retardant BPA thermoset polymer (MP4)

Video of the combustion process of the fiber reinforced BPA composites (MP4)

■ AUTHOR INFORMATION

Corresponding Author

Guoqiang Li − *Department of Mechanical & Industrial Engineering, Louisiana State University, Baton Rouge, Louisiana 70803, United States;* orcid.org/0000-0002-7004-6659; Phone: 001-225-578-5302; Email: lguoqi1@lsu.edu

Author

Xiaming Feng − *Department of Mechanical & Industrial Engineering, Louisiana State University, Baton Rouge, Louisiana 70803, United States*

Complete contact information is available at: https://pubs.acs.org/10.1021/acsami.0c18852

Notes

The authors declare no competing financial interest.

■ ACKNOWLEDGMENTS

This work was supported by the US National Science Foundation under Grant OIA-1946231 and the Louisiana Board of Regents for the Louisiana Materials Design Alliance (LAMDA), National Science Foundation under Grant 1736136, and NASA cooperative agreement NNX16AQ93A under Contract NASA/LEQSF(2016-19)-Phase3-10.

■ REFERENCES

(1) Zhang, B.; Kowsari, K.; Serjouei, A.; Dunn, M. L.; Ge, Q. Reprocessable Thermosets for Sustainable Three-Dimensional Printing. *Nat. Commun.* **2018**, *9*, 1831.

(2) Li, A.; Fan, J. Z.; Li, G. Q. Recyclable Thermoset Shape Memory Polymers with High Stress and Energy Output via Facile UV-Curing. *J. Mater. Chem. A* **2018**, *6* (24), 11479−11487.

(3) Wang, C.; Goldman, T. M.; Worrell, B. T.; McBride, M. K.; Alim, M. D.; Bowman, C. N. Recyclable and Repolymerizable Thiol-X Photopolymers. *Mater. Horiz.* **2018**, *5* (6), 1042−1046.

(4) Zhu, S. W.; Shi, W. F. Flame Retardant Mechanism of Hyperbranched Polyurethane Acrylates Used for UV Curable Flame Retardant Coatings. *Polym. Degrad. Stab.* **2002**, *75* (3), 543−547.

(5) Malucelli, G.; Barbalini, M. UV-Curable Acrylic Coatings Containing Biomacromolecules: A New Fire Retardant Strategy for Ethylene-Vinyl Acetate Copolymers. *Prog. Org. Coat.* **2019**, *127*, 330−337.

(6) Denissen, W.; Winne, J. M.; Du Prez, F. E. Vitrimers: Permanent Organic Networks with Glass-Like Fluidity. *Chem. Sci.* **2016**, *7* (1), 30−38.

(7) Van Zee, N. J.; Nicolay, R. Vitrimers: Permanently Crosslinked Polymers with Dynamic Network Topology. *Prog. Polym. Sci.* **2020**, *104*, 101233.

(8) Gandini, A. The Furan/Maleimide Diels-Alder Reaction: A Versatile Click-Unclick Tool in Macromolecular Synthesis. *Prog. Polym. Sci.* **2013**, *38* (1), 1−29.

(9) Denissen, W.; Rivero, G.; Nicolay, R.; Leibler, L.; Winne, J. M.; Du Prez, F. E. Vinylogous Urethane Vitrimers. *Adv. Funct. Mater.* **2015**, *25* (16), 2451−2457.

(10) Obadia, M. M.; Mudraboyina, B. P.; Serghei, A.; Montarnal, D.; Drockenmuller, E. Reprocessing and Recycling of Highly Cross-Linked Ion-Conducting Networks through Transalkylation Exchanges of C-N Bonds. *J. Am. Chem. Soc.* **2015**, *137* (18), 6078−6083.

(11) Chao, A.; Negulescu, J.; Zhang, D. H. Dynamic Covalent Polymer Networks Based on Degenerative Imine Bond Exchange: Tuning the Malleability and Self-Healing Properties by Solvent. *Macromolecules* **2016**, *49* (17), 6277−6284.

(12) Ruiz de Luzuriaga, A.; Martin, R.; Markaide, N.; Rekondo, A.; Cabanero, G.; Rodriguez, J.; Odriozola, I. Epoxy Resin with Exchangeable Disulfide Crosslinks to Obtain Reprocessable, Repairable and Recyclable Fiber-Reinforced Thermoset Composites. *Mater. Horiz.* **2016**, *3* (3), 241−247.

(13) Zhang, B. R.; Digby, Z. A.; Flum, J. A.; Chakma, P.; Saul, J. M.; Sparks, J. L.; Konkolewicz, D. Dynamic Thiol-Michael Chemistry for Thermoresponsive Rehealable and Malleable Networks. *Macromolecules* **2016**, *49* (18), 6871−6878.

(14) Montarnal, D.; Capelot, M.; Tournilhac, F.; Leibler, L. Silica-Like Malleable Materials from Permanent Organic Networks. *Science* **2011**, *334* (6058), 965−968.

(15) Lu, Y. X.; Tournilhac, F.; Leibler, L.; Guan, Z. B. Making Insoluble Polymer Networks Malleable via Olefin Metathesis. *J. Am. Chem. Soc.* **2012**, *134* (20), 8424−8427.

(16) Rottger, M.; Domenech, T.; van der Weegen, R.; Breuillac, A.; Nicolay, R.; Leibler, L. High-Performance Vitrimers from Commodity Thermoplastics through Dioxaborolane Metathesis. *Science* **2017**, *356* (6333), 62−65.

(17) Yuan, J. S.; Xiong, W.; Zhou, X. H.; Zhang, Y.; Shi, D.; Li, Z. C.; Lu, H. 4-Hydroxyproline-Derived Sustainable Polythioesters: Controlled Ring-Opening Polymerization, Complete Recyclability, and Facile Functionalization. *J. Am. Chem. Soc.* **2019**, *141* (12), 4928−4935.
(18) Nishimura, Y.; Chung, J.; Muradyan, H.; Guan, Z. B. Silyl Ether as a Robust and Thermally Stable Dynamic Covalent Motif for Malleable Polymer Design. *J. Am. Chem. Soc.* **2017**, *139* (42), 14881−14884.
(19) Wang, S.; Ma, S. Q.; Li, Q.; Yuan, W. C.; Wang, B. B.; Zhu, J. Robust, Fire-Safe, Monomer-Recovery, Highly Malleable Thermosets from Renewable Bioresources. *Macromolecules* **2018**, *51* (20), 8001−8012.
(20) Feng, X. M.; Fan, J. Z.; Li, A.; Li, G. Q. Multireusable Thermoset with Anomalous Flame-Triggered Shape Memory Effect. *ACS Appl. Mater. Interfaces* **2019**, *11* (17), 16075−16086.
(21) Lonnberg, H. Cleavage of RNA Phosphodiester Bonds by Small Molecular Entities: A Mechanistic Insight. *Org. Biomol. Chem.* **2011**, *9* (6), 1687−1703.
(22) Ren, M. T.; Cheng, Y. R.; Duan, Q.; Zhou, C. Z. Transesterification Reaction and the Repair of Embedded Ribonucleotides in DNA Are Suppressed upon the Assembly of DNA into Nucleosome Core Particles. *Chem. Res. Toxicol.* **2019**, *32* (5), 926−934.
(23) Morrow, J. R.; Buttrey, L. A.; Berback, K. A. Transesterification of a Phosphate Diester by Divalent and Trivalent Metal-Ions. *Inorg. Chem.* **1992**, *31* (1), 16−20.
(24) Tsang, J. S. W.; Neverov, A. A.; Brown, R. S. La^{3+}-Catalyzed Methanolysis of Hydroxypropyl-p-Nitrophenyl Phosphate as a Model for the RNA Transesterification Reaction. *J. Am. Chem. Soc.* **2003**, *125* (6), 1559−1566.
(25) Yoon, H. J.; Heo, J.; Mirkin, C. A. Allosteric Regulation of Phosphate Diester Transesterification Based upon a Dinuclear Zinc Catalyst Assembled via the Weak-Link Approach. *J. Am. Chem. Soc.* **2007**, *129* (46), 14182−14183.
(26) Makiguchi, K.; Satoh, T.; Kakuchi, T. Diphenyl Phosphate as an Efficient Cationic Organocatalyst for Controlled/Living Ring-Opening Polymerization of delta-Valerolactone and epsilon-Caprolactone. *Macromolecules* **2011**, *44* (7), 1999−2005.
(27) Malik, P.; Chakraborty, D. Hydrogen phosphates: Self Initiated Organocatalysts for the Controlled Ring-Opening Polymerization of Cyclic Esters. *Inorg. Chim. Acta* **2013**, *400*, 32−41.
(28) Macdonald, E. K.; Shaver, M. P. Understanding the Phosphoric Acid Catalysed Ring Opening Polymerisation of B-Butyrolactone and Other Cyclic Esters. *Eur. Polym. J.* **2017**, *95*, 702−710.
(29) Troitzsch, J. Flame-Retardant Polymers Current Status and Future-Trends. *Makromol. Chem., Macromol. Symp.* **1993**, *74*, 125−135.
(30) Huang, Y. B.; Jiang, S. H.; Liang, R. C.; Sun, P.; Hai, Y.; Zhang, L. Thermal-Triggered Insulating Fireproof Layers: A Novel Fire-Extinguishing Mxene Composites Coating. *Chem. Eng. J.* **2020**, *391*, 123621.
(31) Feng, X. M.; Wang, X.; Cai, W.; Hong, N. N.; Hu, Y.; Liew, K. M. Integrated Effect of Supramolecular Self-Assembled Sandwich-Like Melamine Cyanurate/MoS_2 Hybrid Sheets on Reducing Fire Hazards of Polyamide 6 Composites. *J. Hazard. Mater.* **2016**, *320*, 252−264.
(32) Mauerer, O. New Reactive, Halogen-Free Flame Retardant System for Epoxy Resins. *Polym. Degrad. Stab.* **2005**, *88* (1), 70−73.
(33) Wang, X.; Zhou, S.; Guo, W. W.; Wang, P. L.; Xing, W. Y.; Song, L.; Hu, Y. Renewable Cardanol-Based Phosphate as a Flame Retardant Toughening Agent for Epoxy Resins. *ACS Sustainable Chem. Eng.* **2017**, *5* (4), 3409−3416.
(34) Huang, Y. B.; Jiang, S. H.; Liang, R. C.; Liao, Z. W.; You, G. X. A Green Highly-Effective Surface Flame-Retardant Strategy for Rigid Polyurethane Foam: Transforming UV-Cured Coating into Intumescent Self-Extinguishing Layer. *Composites, Part A* **2019**, *125*, 105534.
(35) Wu, M.; Yuan, L.; Jiang, F.; Zhang, Y.; He, Y.; You, Y.-Z.; Tang, C.; Wang, Z. Strong Autonomic Self-Healing Biobased Polyamide Elastomers. *Chem. Mater.* **2020**, *32* (19), 8325−8332.
(36) Gong, H. R.; Gao, Y. J.; Jiang, S. L.; Sun, F. Photocured Materials with Self-Healing Function through Ionic Interactions for Flexible Electronics. *ACS Appl. Mater. Interfaces* **2018**, *10* (31), 26694−26704.
(37) Li, X. P.; Yu, R.; He, Y. Y.; Zhang, Y.; Yang, X.; Zhao, X. J.; Huang, W. Four-Dimensional Printing of Shape Memory Polyurethanes with High Strength and Recyclability Based on Diels-Alder Chemistry. *Polymer* **2020**, *200*, 122532.
(38) Li, A.; Challapalli, A.; Li, G. Q. 4D Printing of Recyclable Lightweight Architectures Using High Recovery Stress Shape Memory Polymer. *Sci. Rep.* **2019**, *9*, 7621.
(39) Wang, S. P.; Wu, Y. G.; Dai, J. Y.; Teng, N.; Peng, Y. Y.; Cao, L. J.; Liu, X. Q. Making Organic Coatings Greener: Renewable Resource, Solvent-Free Synthesis, UV Curing and Repairability. *Eur. Polym. J.* **2020**, *123*, 109439.
(40) Li, C.; Liu, J. W.; Chen, Y. Z.; Li, T.; Cai, X. X.; Sung, J. G.; Sun, X. Z. S. S. Hybrid Network via Instantaneous Photoradiation: High Efficient Design of 100% Bio-Based Thermosets with Remoldable and Recyclable Capabilities after UV Curing. *Chem. Eng. J.* **2018**, *336*, 54−63.
(41) Wang, S. P.; Teng, N.; Dai, J. Y.; Liu, J. K.; Cao, L. J.; Zhao, W. W.; Liu, X. Q. Taking Advantages of Intramolecular Hydrogen Bonding to Prepare Mechanically Robust and Catalyst-Free Vitrimer. *Polymer* **2020**, *210*, 123004.
(42) Podgorski, M.; Mavila, S.; Huang, S. J.; Spurgin, N.; Sinha, J.; Bowman, C. N. Thiol-Anhydride Dynamic Reversible Networks. *Angew. Chem., Int. Ed.* **2020**, *59* (24), 9345−9349.
(43) Ogden, W. A.; Guan, Z. B. Recyclable, Strong, and Highly Malleable Thermosets Based on Boroxine Networks. *J. Am. Chem. Soc.* **2018**, *140* (20), 6217−6220.
(44) Taynton, P.; Yu, K.; Shoemaker, R. K.; Jin, Y. H.; Qi, H. J.; Zhang, W. Heat- or Water-Driven Malleability in a Highly Recyclable Covalent Network Polymer. *Adv. Mater.* **2014**, *26* (23), 3938−3942.
(45) Snyder, R. L.; Fortman, D. J.; De Hoe, G. X.; Hillmyer, M. A.; Dichtel, W. R. Reprocessable Acid-Degradable Polycarbonate Vitrimers. *Macromolecules* **2018**, *51* (2), 389−397.
(46) Fortman, D. J.; Brutman, J. P.; Cramer, C. J.; Hillmyer, M. A.; Dichtel, W. R. Mechanically Activated, Catalyst-Free Polyhydroxyurethane Vitrimers. *J. Am. Chem. Soc.* **2015**, *137* (44), 14019−14022.
(47) Kim, E.; Yang, J.; Choi, J.; Suh, J. S.; Huh, Y. M.; Haam, S. Synthesis of Gold Nanorod-Embedded Polymeric Nanoparticles by a Nanoprecipitation Method for Use as Photothermal Agents. *Nanotechnology* **2009**, *20* (36), 365602.
(48) Heredia-Guerrero, J. A.; San-Miguel, M. A.; Luna, M.; Dominguez, E.; Heredia, A.; Benitez, J. J. Structure and Support Induced Structure Disruption of Soft Nanoparticles Obtained from Hydroxylated Fatty Acids. *Soft Matter* **2011**, *7* (9), 4357−4363.
(49) Nifant'ev, I. E.; Shlyakhtin, A. V.; Tavtorkin, A. N.; Kosarev, M. A.; Gavrilov, D. E.; Komarov, P. D.; Ilyin, S. O.; Karchevsky, S. G.; Ivchenko, P. V. Mechanistic Study of Transesterification in TBD-Catalyzed Ring-Opening Polymerization of Methyl Ethylene Phosphate. *Eur. Polym. J.* **2019**, *118*, 393−403.
(50) Alongi, J.; Carletto, R. A.; Di Blasio, A.; Carosio, F.; Bosco, F.; Malucelli, G. DNA: A Novel, Green, Natural Flame Retardant and Suppressant For Cotton. *J. Mater. Chem. A* **2013**, *1* (15), 4779−4785.
(51) Feng, X. M.; Wang, X.; Cai, W.; Qiu, S. L.; Hu, Y.; Liew, K. M. Studies on Synthesis of Electrochemically Exfoliated Functionalized Graphene and Polylactic Acid/Ferric Phytate Functionalized Graphene Nanocomposites as New Fire Hazard Suppression Materials. *ACS Appl. Mater. Interfaces* **2016**, *8* (38), 25552−25562.
(52) Sheng, X. X.; Li, S. H.; Zhao, Y. F.; Zhai, D. S.; Zhang, L.; Lu, X. Synergistic Effects of Two-Dimensional MXene and Ammonium Polyphosphate on Enhancing the Fire Safety of Polyvinyl Alcohol Composite Aerogels. *Polymers* **2019**, *11* (12), 1964.

https://dx.doi.org/10.1021/acsami.0c18852
ACS Appl. Mater. Interfaces 2020, 12, 57486−57496